2014

Structural, magnetic, and electron transport properties of $Mn_{3-x}Pt_xSn$ (x = 0, 0.5, 1) nanomaterials

A Nelson
South Dakota State University, University of Nebraska-Lincoln

Yung Huh
South Dakota State University, University of Nebraska-Lincoln, yung.huh@sdstate.edu

Parashu Kharel
South Dakota State University, University of Nebraska-Lincoln, pkharel2@unl.edu

Shah R. Valloppilly
University of Nebraska-Lincoln, svalloppilly2@unl.edu

Ralph A. Skomski
University of Nebraska-Lincoln, rskomski2@unl.edu

See next page for additional authors

Structural, magnetic, and electron transport properties of $Mn_{3-x}Pt_xSn$ (x = 0, 0.5, 1) nanomaterials

A. Nelson,[1,2] Y. Huh,[1,2] P. Kharel,[1,2,a)] V. R. Shah,[2] R. Skomski,[2,3] and D. J. Sellmyer[2,3]
[1]*Department of Physics, South Dakota State University, Brookings, South Dakota 57007, USA*
[2]*Nebraska Center for Materials and Nanoscience, University of Nebraska, Lincoln, Nebraska 68588, USA*
[3]*Department of Physics and Astronomy, University of Nebraska, Lincoln, Nebraska 68588, USA*

(Presented 5 November 2013; received 21 September 2013; accepted 13 November 2013; published online 21 February 2014)

The structural, magnetic, and electron-transport properties of $Mn_{3-x}Pt_xSn$ (x = 0, 0.5, 1) nanomaterials prepared by arc-melting, melt-spinning, and annealing were investigated. It was found that the hexagonal structure is the most stable structure for Mn_3Sn and the samples show an antiferromagnetic spin order at room temperature. The Pt-containing samples are mainly tetragonal but contain a small amount of other impurity phases, including hexagonal Mn_3Sn and Mn_2Sn. At room temperature, the Pt-containing samples show ferri- or ferromagnetic spin order with a Curie temperature of about 370 K. The measured high-field magnetization and anisotropy constant for Mn_2PtSn are 405 emu/cm^3 and 2.6 Mergs/cm^3, respectively. The samples are all highly conducting with metallic electron transport and show a substantial negative magnetoresistance. [http://dx.doi.org/10.1063/1.4865977]

I. INTRODUCTION

High-anisotropy magnetic materials with Curie temperatures above room temperature have potential for a range of applications, including permanent magnets, high-density recording, and spintronic devices.[1–3] Current efforts on spintronic devices focus on exploiting the spin transfer torque (STT) phenomena for non-volatile memory and logic devices. An ideal material for STT-based spintronic devices should exhibit high perpendicular anisotropy combined with high spin polarization at the Fermi level and low net magnetization, the latter to minimize field effects.[4] It has been found recently that the Mn-based tetragonal compound $Mn_{3-x}Ga$ ($x = 2$–3) is a promising materials for STT applications.[5,6] However, its large lattice mismatch with MgO and relatively high magnetization are drawbacks. Another Mn-based compound predicted to have high potential for STT application is tetragonal $Mn_{3-x}Y_xSn$ (Y = 4d or 5d elements). Mn_2PtSn is of special interest because of the predicted high magnetocrystalline anisotropy (~50 Mergs/cm^3) and high spin polarization ($P = 91\%$) at the Fermi level.[7,8]

Mn_3Sn has been predicted to exist in both hexagonal $D0_{19}$ and tetragonal $D0_{22}$ crystal structures; however, only the hexagonal phase ($a = 5.665$ Å, $c = 4.531$ Å) has been synthesized in experiment.[9] At room temperature, the hexagonal Mn_3Sn exhibits a triangular antiferromagnetic order, where the Mn-sublattice magnetizations lie in the plane perpendicular to the hexagonal basal plane resulting in zero net magnetization.[10] On the other hand, Mn_2PtSn can be synthesized in an inverse tetragonal crystal structure with ferromagnetic spin order at room temperature. Because of the high magnetic anisotropy, low magnetization, and high spin polarization at the Fermi level, this material is expected to be promising for STT applications. Here, we present our experimental results on $Mn_{3-x}Pt_xSn$ (x = 0, 0.5, 1) nanomaterial. Our interest is to understand how structural, magnetic, and electron transport properties of $Mn_{3-x}Pt_xSn$ change with changing Pt content.

II. EXPERIMENTAL METHODS

The $Mn_{3-x}Pt_xSn$ (x = 0, 0.5, 1) ribbons were prepared using arc-melting, melt-spinning, and annealing. The nanostructured ribbons were produced by rapidly quenching the induction melted $Mn_{3-x}Pt_xSn$ onto the surface of a rotating copper wheel in a highly pure argon filled chamber. The ribbons were about 1 mm wide and 85 μm thick. The wheel was kept at the tangential speed of 20 m/s for all samples. In order to investigate the effect of annealing on the crystal structure, the ribbons were annealed in a tubular vacuum furnace with a base pressure of about 10^{-7} Torr at a temperature of 300 °C, 450 °C, and 600 °C for up to 50 h. The elemental compositions were confirmed using energy dispersive x-ray spectroscopy (EDX), which showed that the compositions were close to the estimated values within an error of 0.1 at. %. The structural properties of the samples were studied by x-ray diffraction (XRD) using a Rigaku D/Max-B x-ray diffractometer with cobalt source. The magnetic and electron transport properties were investigated with a Quantum Design SQUID magnetometer and a Physical Properties Measurement System (PPMS). The Rietveld analysis of the x-ray diffraction patterns was done using TOPAS software.[11]

III. RESULTS AND DISCUSSION

Figure 1(a) shows the x-ray diffraction patterns for the Mn_3Sn, $Mn_{2.5}Pt_{0.5}Sn$, and Mn_2PtSn ribbons. We found that the rapidly quenched Mn_3Sn ribbons prefer the hexagonal structure. We tried different annealing times and temperatures (up to 600 °C and 100 h) to see if there would be a transition from the hexagonal to the tetragonal structure but the ribbons

a)Electronic mail: parashu.kharel@sdstate.edu.

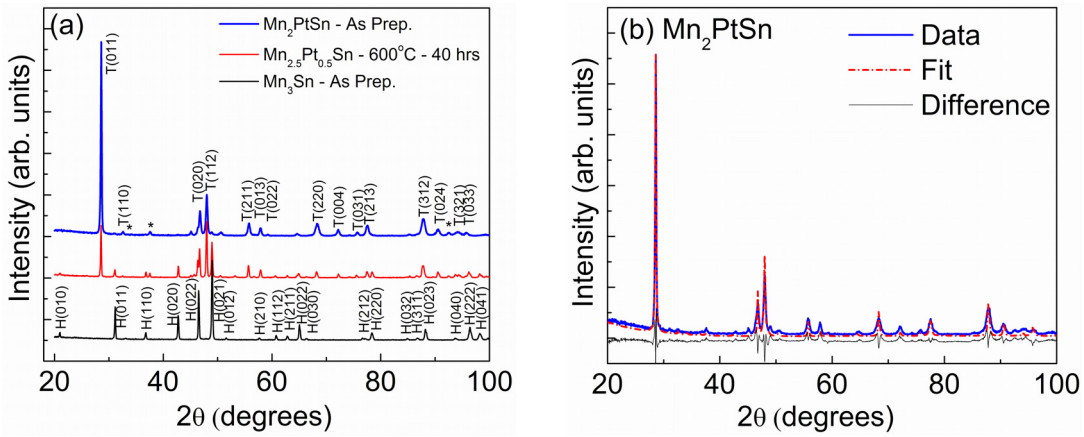

FIG. 1. (a) Experimental XRD patterns for Mn_3Sn, $Mn_{2.5}Pt_{0.5}Sn$, and Mn_2PtSn melt-spun ribbons, where H, T, and * corresponds to the hexagonal Mn_3Sn, inverse tetragonal Mn_2PtSn, and hexagonal Mn_2Sn phases, respectively; (b) simulated power x-ray diffraction pattern (Rietveld plot) corresponding to the inverse tetragonal structure of Mn_2PtSn alloy, compared with experimental data shown in blue color.

remained hexagonal, regardless of different annealing conditions. Once Pt was added, the preferred structure transformed from hexagonal to inverse tetragonal but the samples still contained some hexagonal Mn_3Sn. Rietveld refinement of x-ray diffraction patterns shows that the amount of hexagonal Mn_3Sn phase decreases with increasing Pt content.

Figure 1(b) compares a simulated powder diffraction pattern for inverse tetragonal Mn_2PtSn alloy with the experimental data. The intensities and 2θ positions of most of the diffraction peaks in the experimental pattern show a very close match with the simulated pattern. However, the refinement also indicates that the sample contains a small amount of secondary phases (about 8 wt. % Mn_2Sn and about 7 wt. % Mn_3Sn). The Rietveld-refined lattice parameters for Mn_2PtSn are $a = 4.201$ Å and $c = 5.553$ Å with $c/a = 1.32$. All the samples were polycrystalline; however, some preferred texture was detected as commonly observed in the melt-spun ribbons. Both Pt-containing samples ($Mn_{2.5}Pt_{0.5}Sn$ and Mn_2PtSn) were annealed at various temperatures to obtain single phase $Mn_{3-x}Pt_xSn$. We found that an optimum annealing condition, which significantly reduced the Mn_3Sn phase in $Mn_{2.5}Pt_{0.5}Sn$, was 600 °C for 40 h. We believe that a longer annealing time is required to completely eliminate the hexagonal impurities in both $Mn_{2.5}Pt_{0.5}Sn$ and Mn_2PtSn ribbons.

Figure 2 shows the magnetic-field dependence of magnetizations of $Mn_{3-x}Pt_xSn$ ribbons measured at room temperature. As shown in the inset of Fig. 2, the $M(H)$ curve of Mn_3Sn is almost linear but shows a clearly open hysteresis loop near the origin. The high-field ($H = 70$ kOe) magnetization and coercivity are about 1.8 emu/g and 5 kOe, respectively. However, the samples containing Pt show completely different magnetic properties, where the $M(H)$ loops are almost saturated and have small coercivities (~0.5 kOe) consistent with soft ferromagnetic behavior. The measured high-field ($H = 70$ kOe) magnetizations for $Mn_{2.5}Pt_{0.5}Sn$ and Mn_2PtSn are 24 emu/g and 36 emu/g (405 emu/cm^3), respectively. We have used the density of a stoichiometric Mn_2PtSn (11.43 g/cm^3) to express the magnetization into emu/cm^3, although the real density of our Mn_2PtSn sample should be slightly smaller than this value because of the presence of secondary phases.

The anisotropy energies of $Mn_{2.5}Pt_{0.5}Sn$ and Mn_2PtSn were determined using the approach to saturation method.[6,12] We have found that both Pt-containing samples show high magnetic anisotropy on the order of 10^6 ergs/cm^3 (2.6 Mergs/cm^3 for Mn_2PtSn). This value of anisotropy energy is about one order smaller than the theoretically predicted value of about 50 Mergs/cm^3 for Mn_2PtSn. We note that the observed coercivity of the Mn_2PtSn ribbon does not scale with the anisotropy energy. Since coercivity is an extrinsic magnetic property which depends on the microstructure and texture of a sample, we do not expect the coercivity of these polycrystalline ribbons to scale with their anisotropy energy.

Figure 3 shows the temperature dependence of magnetizations $M(T)$ of $Mn_{3-x}Pt_xSn$ ribbons between 10 K and 500 K. The samples were first cooled at 1 kOe and magnetizations were measured at the same field while the temperature gradually increased from 10 K to 400 K. For high temperature measurement (from 300 K to 500 K), samples were mounted on a VSM oven heater stick and measured separately. As shown in the inset of Fig. 3, the $M(T)$ curve exhibits an increase in magnetizations near 70 K, 260 K, and 430 K. These anomalies in magnetizations are consistent with neutron diffraction results reported in the

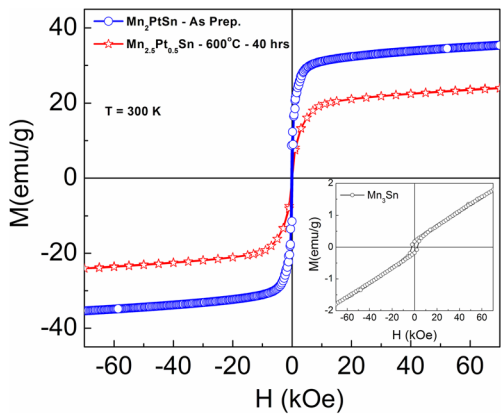

FIG. 2. The magnetic field dependence of the magnetizations for the Mn_2PtSn and $Mn_{2.5}Pt_{0.5}Sn$ ribbons, measured at room temperature. The inset shows the $M(H)$ hysteresis curve for the rapidly quenched Mn_3Sn ribbon.

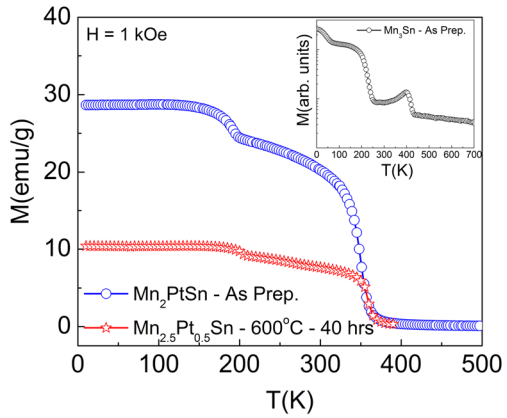

FIG. 3. The temperature dependence of magnetizations $M(T)$ for Mn_2PtSn and $Mn_{2.5}Pt_{0.5}Sn$ ribbons measured at $H = 1$ kOe. The inset shows the $M(T)$ curve for rapidly quenched Mn_3Sn ribbon measured at 1 kOe. We note that the vertical scale of the inset is logarithmic.

literatures.[10,13] The anomaly near 420 K corresponds to the Néel temperature. The room-temperature M(H) curve for Mn_3Sn sample shows a signature of a weak ferromagnetism. According to neutron diffraction studies, the onset of weak ferromagnetism, which also occurs near 420 K, is a consequence of a slight distortion in the triangular magnetic structure due to anisotropy energy.[10,13] The upturn in magnetization as temperature decreases below 260 K has been attributed to the transition to a helical magnetic structure. The increase in magnetization below 70 K has been interpreted as the result of a shift of the sublattice magnetization plane to a position parallel to the basal plane.[10] On the other hand, the magnetizations of both Pt-containing samples show clear magnetic transitions near 200 K and 370 K. The magnetic transition at 370 K is consistent with the predicted Curie temperature ($T_c = 374$ K) of Mn_2PtSn.[7] Since our samples contain a small amount of Mn_2Sn and the Curie temperature of ferromagnetic Mn_2Sn is close to 200 K, the transition near 200 K can be explained by the presence of Mn_2Sn.

The temperature dependences $R(T)$ of electrical resistance of the $Mn_{3-x}Pt_xSn$ ribbons between 5 K and 300 K are shown in Fig. 4. The resistances were measured while the temperature gradually increased from 5 K to 300 K, using a four-point-probe method. As shown in Fig. 4, the resistances are normalized to the value at 5 K for better comparison. All the samples are highly conducting and show typical metallic behavior between 5 K and 200 K, where the temperature coefficient of resistance is positive. However, the $R(T)$ curves show a change in the slope as the temperature increases above 200 K. We believe that the change in slopes of the $R(T)$ curves is linked to the magnetic transition observed in these samples. The residual resistances are in the range of milliohms (resistivity at 5 K ~ 1.2 mΩ cm for Mn_3Sn and 2.6 mΩ cm for Mn_2PtSn). The residual resistance ratio (RRR) defined as $R_{300\,K}/R_{5\,K}$ is 3.5 for Mn_3Sn, which decreases with increasing Pt concentration and reaches 2 for Mn_2PtSn. This indicates that Pt-containing samples have high structural disorder and/or defect concentration. This may be caused by the structural transformation of Pt-containing samples from hexagonal to tetragonal phase without complete elimination of the hexagonal impurities. We have found that all three samples show a substantial negative magnetoresistance (3.7% for Mn_2PtSn and 3.1% for Mn_3Sn at 5 K with $H = 50$ kOe) but without any change in the shape of the $R(T)$ curves.

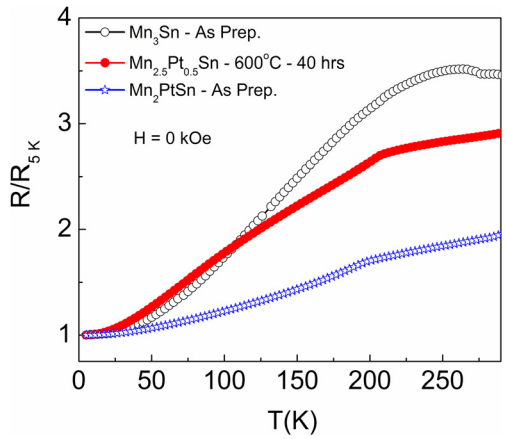

FIG. 4. Normalized resistances ($R/R_{5\,K}$) as a function of temperature for $Mn_{3-x}Pt_xSn$ ($x = 0$, 0.5, 1) ribbons. The resistances were measured between 5 K and 300 K at zero magnetic field.

IV. CONCLUSIONS

We have prepared $Mn_{3-x}Pt_xSn$ (x = 0, 0.5, 1) nanomaterials using arc-melting, melt-spinning, and annealing. The rapidly quenched hexagonal Mn_3Sn ribbons are antiferromagnetic at room temperature but show interesting magnetic transitions as the temperature decreases below 300 K. The Pt-containing samples, $Mn_{2.5}Pt_{0.5}Sn$ and Mn_2PtSn, are mainly inverse tetragonal in structure and show ferro- (or ferrimagnetic) behavior at room temperature. All samples have small residual resistances in the order of milliohms-cm and are metallic. Although Mn_2PtSn has relatively low magnetization and high magnetic anisotropy, its low Curie temperature is an obstacle for technological applications and it is necessary to address this issue before it can be used for devices. Also, it is important to investigate the degree of spin polarization in thin films of this material to determine if this material is useful for STT-based devices.

ACKNOWLEDGMENTS

This research was supported by NSF-MRSEC (DMR-0820521). We would like to thank J. E. Shield for allowing us to use his sample-preparation facility.

[1]C. Chappert *et al.*, Nature Mater. **6**, 813 (2007).
[2]R. Sbiaa *et al.*, Phys. Status Solidi RRL **5**, 413 (2011).
[3]R. Skomski and J. M. D. Coey, *Permanent Magnetism* (Institute of Physics Publishing, Bristol, 1998).
[4]H. Kurt *et al.*, Phys. Status Solidi B **248**, 2338 (2011).
[5]B. Balke *et al.*, Appl. Phys. Lett. **90**, 152504 (2007).
[6]Y. Huh *et al.*, IEEE Trans. Magn. **49**, 3277 (2013).
[7]J. Winterlik *et al.*, Adv. Mater. **24**, 6283 (2012).
[8]J. Kübler and C. Felser, Phys. Rev. B **85**, 012405 (2012).
[9]D. Zhang *et al.*, J. Phys.: Condens. Matter **25**, 206006 (2013).
[10]T. Nagamiya, J. Phys. Soc. Jpn. **46**, 787 (1979).
[11]TOPAS-V 4.2, Bruker AXS, Inc.
[12]G. Hadjipanayis and D. J. Sellmyer, Phys. Rev. B **23**, 3349 (1981).
[13]P. J. Brown *et al.*, J. Phys.: Condens. Matter **2**, 9409 (1990).